BOLLETTINO DI GEOFISICA TEORICA ED APPLICATA VOL. XXXVII, N. 145 - MARCH 1995

G. BOEHM, A. CAMERLENGHI, E. LODOLO and A. VESNAVER

TOMOGRAPHIC ANALYSIS AND GEOLOGICAL CONTEXT OF A BOTTOM SIMULATING REFLECTOR ON THE SOUTH SHETLAND MARGIN (ANTARCTIC PENINSULA)

Abstract. A seismic reflection tomographic analysis to identify spatial variations of wave velocity across a Bottom Simulating Reflector (BSR) on the South Shetland Margin, in the northern tip of the Antarctic Peninsula is presented. The resolving power of the acquired seismic data is quantified in order to evaluate the reliability of the velocity analyses performed. We show that conventional and continuous velocity spectra, as well as tomographic inversion of reflected arrivals, support the hypothesis that the strong reflector is due to the presence of a gas hydrate layer overlying a zone of free gas. The hydrate layer is characterized by lateral variations of the average interval velocity over the range 2000 to 2200 m/s. The gas-bearing sediments are identified in a continuous low-velocity zone of average interval velocity in the range 1500 m/s $\pm$ 10%, between the BSR and the first detectable reflector picked about 80 ms below it. The resolution of the acquisition system or of the tomographic inversion does not allow us to identify the actual thickness of the predicted gas-bearing layer. A geological framework for the South Shetland Margin and a general overview of the relevance of gas hydrates in geological processes are presented as an introduction to the tomographic analysis.

INTRODUCTION

Hydrates of natural gases have attracted increasing attention for the scientific community because of their implication in the geological evolution of continental margins and their potential for understanding global changes in the Earth's climate (see e.g. Kvenvolden, 1993).

Since hydrates are composed mainly of methane and water, and since the warming potential of methane is much higher than that of carbon dioxide, the release of large amounts of methane into the atmosphere as a consequence of submarine hydrate sublimation could have affected the Earth global climate in the past through the "greenhouse" effect.

The clearest evidence for the presence of a gas hydrate layer in the sub-bottom is a characteristic "Bottom Simulating Reflector" (BSR), which appears on marine seismic reflection profiles. This phenomenon is observed worldwide along the continental slopes and rises of most continental margins.

A prominent gas hydrate bottom simulating reflector was identified on some seismic reflection profiles acquired by the Osservatorio Geofisico Sperimentale during the 1989/90 Antarctic Survey in the South Shetland Margin of the Antarctic Peninsula (Lodolo et al., 1993). A 3000 m long streamer was used, with 120-channels and a group spacing of 25 m. The energy source was a 45 litre airgun array with shot interval of 50 m, so that the coverage was 30-fold, the sampling interval was 4 ms.

Manuscript received, January 4, 1994; accepted May 5, 1994.

Osservatorio Geofisico Sperimentale, P.O. Box 2011, 34016 Trieste, Italy.

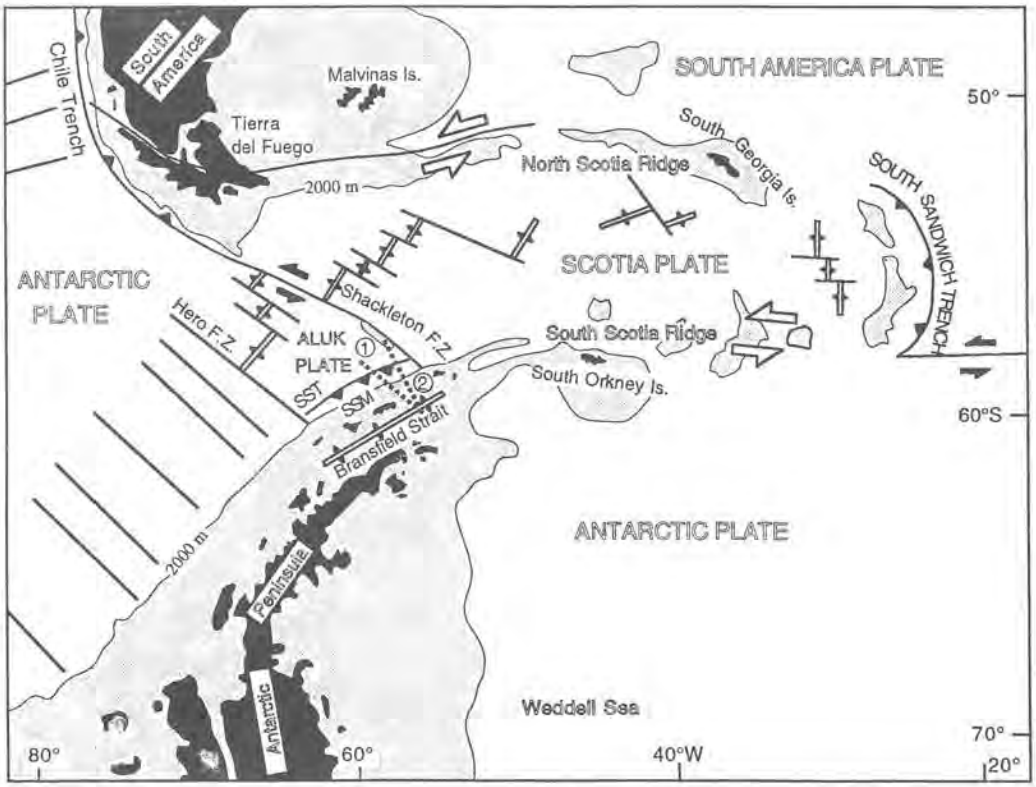

Fig. 1 - Tectonic map of the Antarctic Peninsula with the main geological structures. SST = South Shetland Trench; SSM = South Shetland Margin; 1 = Line IT9044; 2 = Line IT9043.

The BSR was initially recognized on stacked sections obtained by a standard processing sequence (Lodolo e Camerlenghi, 1992; Lodolo et al., 1993; Camerlenghi and Lodolo, 1994).

In this paper we present the results of a tomographic analysis of this reflector aimed at resolving better the velocity structure across the BSR, to get a further seismic evidence of the presence of free gas. The algorithm adopted is based on the dual tomography (Carrion, 1991; Carrion et al., 1993a, 1993b), and provides an accurate reconstruction of the local velocity distribution and reflector position in depth from conventional surface seismic data.

GEOLOGICAL SETTING

The South Shetland Margin belongs to a wide and complex continental margin (Pacific Margin of the Antarctic Peninsula), which extends approximately from the Bellingshausen Sea to the tip of the Antarctic Peninsula in the Drake Passage (Fig. 1).

The complexity of the Pacific Margin of the Antarctic Peninsula is due to a long tectonic history of axial ridge crest-trench collision that progressed from the SW to the NE, from the Eocene (50 Ma) until the Pliocene (4 Ma). Such a unique evolution was identified initially from the distribution of magnetic anomalies on the oceanic floor (Barker, 1982), and later from the interpretation of multichannel seismic profiles and gravity modelling (Larter and Barker, 1991). According to Hawkes (1981), the boundaries between the segments of oceanic crust (fracture zones) are reflected in the continental crust of the northern Antarctic Peninsula by transverse megafractures, which affect the distribution of volcanic land provinces and the outcrop of pre-Jurassic basement.

The South Shetland Margin occupies the NE part of the Pacific Margin of the Antarctic Peninsula, and is limited by the Hero Fracture Zone to the SW and by the Shackleton Fracture Zone to the NE. It shows the typical features of an active (convergent) margin:

1) *Aluk (or Phoenix) oceanic ridge.* The ridge is identified by the symmetry of marine magnetic anomalies across its axis. The youngest is Anomaly 3 (4.5 Ma), which is about 30 km from the ridge axis (Larter and Barker, 1991). Data closer to the axis do not allow univocal identification of younger anomalies. Although the ridge is commonly believed to have ceased spreading about 4 Ma ago (it should thus be considered inactive), an extremely low spreading rate may have persisted until more recent times.

2) *South Shetland Trench.* A well developed subduction trench is present along the entire South Shetland Margin (Fig. 2). The oceanic side of the trench is characterised by normal faulting in the basement, which produces a marked horst-and-graben tectonic style. A deep graben is imaged right in the trench, where a well developed reverse fault in the oceanic basement is probably related to the vicinity of the Shackleton Fracture Zone and to a diffuse intraplate stress field (Pelayo and Wiens, 1989). The trench sediment fill is composed of two seismic units identified mainly from their frequency/amplitude character. Reflectors are always sub-parallel, with good lateral continuity. The lowest trench-fill unit onlaps the outer, faulted side of a graben.

The inner portion of the trench is characterised by folding and reverse faulting of the sediments. A *décollement* surface can be identified along a strong high amplitude/low frequency reflector that merges with the transition between the two units. The reflector that identifies the oceanic basement is clearly visible within the trench and can be followed to at least 10 km below the continental slope.

3) *South Shetland Accretionary Prism and Fore-Arc Basin.* A wedge of accreted sediments is identified on the continental slope by the presence of a unit of incoherent seismic response. Chaotic reflectors alternate with landward-dipping, high amplitude/low frequency reflectors. In the upper portion of the continental slope, a finely layered unit characterised by high frequency reflections overlies the chaotic unit. In the lower part of the slope, reflectors are sub-parallel to the sea floor, while in the upper part they are deformed (with folding, sea floor truncation, and lateral termination of reflectors). This unit is interpreted as part of a fore-arc sedimentary basin that has been affected by the deformation of the accretionary complex. According to various seismic profiles, the fore-arc basin extends under the continental shelf as far as the South Shetland Islands (Gambôa and Maldonado, 1990).

The gas hydrate BSR studied here was found in the accreted and fore-arc basic units along the continental slope of the South Shetland Margin (see Fig 2).

4) *South Shetland Island Arc.* The South Shetland Islands are located on a 32 km thick continental crust (Guterch et al., 1985). They are composed of a thick sequence of calc-alkaline volcanic, volcanoclastic, marine and continental sediments, ranging in age from Jurassic to Tertiary, unconformably overlying a pre-Jurassic meta-sedimentary basement (Gonzàlez-Ferran, 1985). This phase of calc-alkaline magmatism was generated by Cretaceous and Tertiary subduction of oceanic lithosphere under the South Shetland Margin. The absence of volcanic activity after the Miocene supports the idea of cessation (or drastic reduction) of active subduction at the trench.

5) *Bransfield Back-arc Basin.* The Bransfield Strait, located between the South Shetland Islands and the northern part of the Antarctic Peninsula, is a marginal basin with an active spreading centre. Basaltic volcanism is thought to have started at 2-3 Ma in response to the onset of a tectonic rifting phase (Gambôa and Maldonado, 1990) that followed cessation (or decrease) of spreading at the Aluk Ridge.

From this it emerges that all the elements of a classic active margin where oceanic lithosphere is subducted under a continental island arc are present along the South Shetland Margin. Barker (1982) and Larter and Barker (1991) provide the only comprehensive model for the tectonic development of this margin: the tectonic activity presently observed in the trench on the accretionary prism and fore-arc basin, and the onset of the extensional regime of the Bransfield Strait, are produced by the gravitational sinking and roll-back of the oceanic lithosphere that

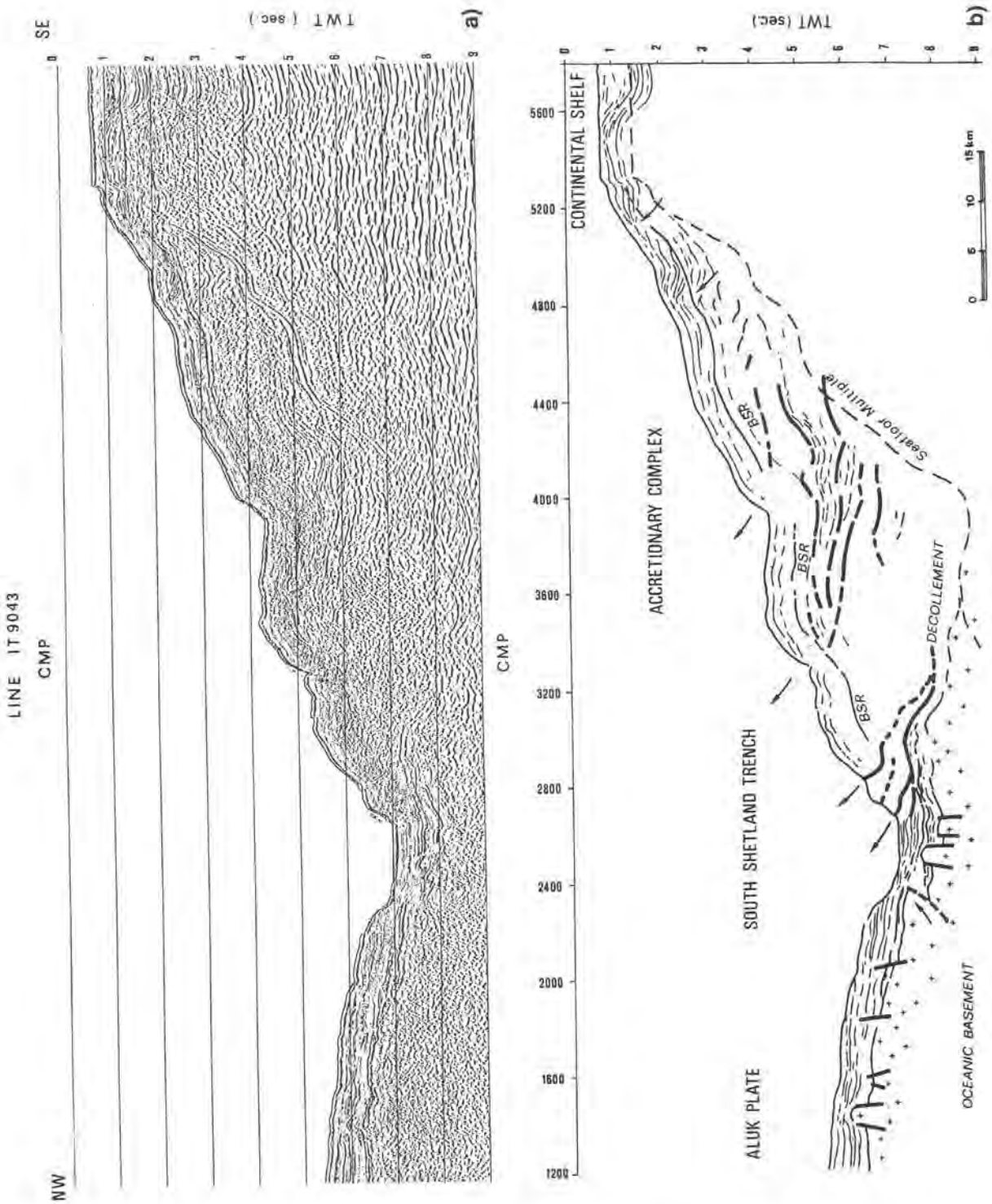

Fig. 2 - (a) Fully processed and migrated seismic profile IT9043 across the South Shetland Margin and trench. (b) Simplified line drawing. Bold lines indicate faults and thrusts. Arrows indicate the direction of tectonic deformation. Note that active deformation is located at the toe of the accretionary prism.

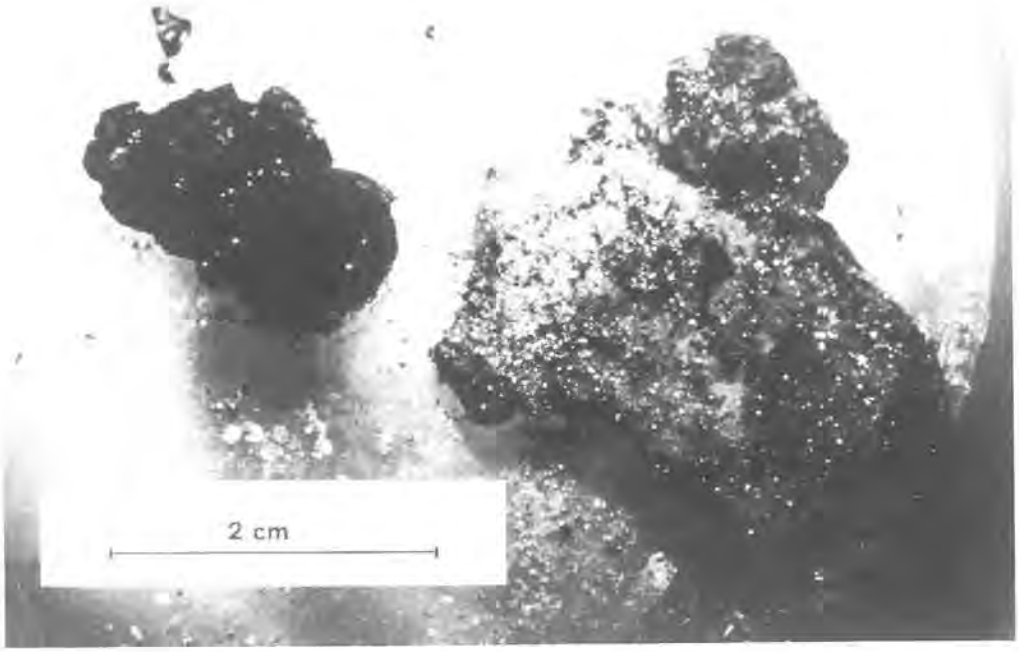

Fig. 3 - A gas hydrate core sample collected by the *R/V Gelendzhic* during the TREDMAR-93 cruise on the mud volcanoes of the Black Sea (courtesy of M. Ivanov; photo by R. Lucchi).

followed the cessation (or marked reduction) of the Aluk ridge spreading (4 Ma).

GAS HYDRATES

For the reader unfamiliar with gas hydrates and bottom simulating reflectors we summarize here the main points regarding their nature. Further details and a comprehensive and exhaustive review on gas hydrates, from a geological and global perspective, can be found in Kvenvolden (1993).

Gas hydrates (a variety of gas clathrates) are natural solid compounds, in which a guest molecule (largely methane) fits into separate nearly spherical chambers within a host molecule (water). There are no ordinary chemical bonds between the atoms of the host molecule and those of the guest molecule.

Gas hydrates resemble ice or wet snow in appearance (Fig. 3), in which water crystallizes in the isometric crystallographic system rather than the hexagonal system of normal ice (see Hitchon, 1974, for a detailed description of gas hydrate structure).

The occurrence of gas hydrates in nature is controlled by pressure-temperature stability conditions and composition, as illustrated by the phase diagram in Fig. 4. In the marine environment, these conditions are met within continental margin sediments at water depths greater than 300 m, and bottom water temperatures approaching 0° C; in continental polar regions, the upper depth limit for methane hydrates is about 150 m, where surface temperatures are below 0° C. The lower limit is determined by the geothermal gradient, about 2000 m below the solid surface. The occurrence of gas hydrates is thus restricted to the shallow geosphere. Because of the pressure-temperature requirements, clathrates are mostly present in polar and deep oceanic regions. In the former, gas hydrates are normally associated with permafrost, both onshore and offshore; in the latter, gas hydrates are found on outer continental margins

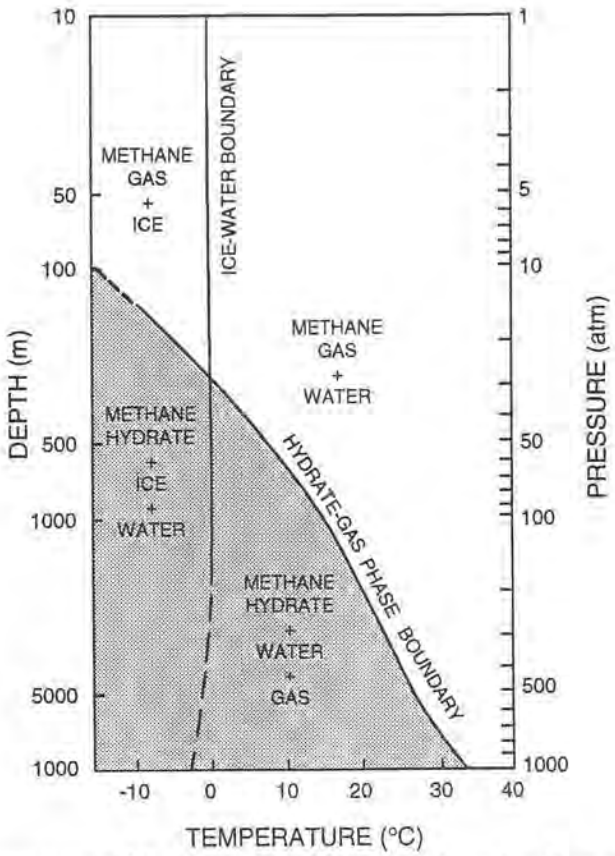

Fig. 4 - Pressure-temperature stability diagram for gas hydrates (redrawn from Kvenvolden, 1993).

in the sediments of slopes and rises where cold bottom water is present.

Only limited information on the nature of the hydrate is available from deep-sea drilling (e.g. subduction zone accretionary sedimentary prisms offshore Central America, western and eastern United States and Japan). Most information on the zone of gas hydrate stability must be inferred from seismic reflection data from the appearance of anomalous bottom simulating reflectors (Shipley et al., 1979; Shipley and Didyk, 1981; Collins and Watkins, 1985; Minshull and White, 1989; Andreassen et al., 1990; Miller et al., 1991; Hyndman and Spence, 1992; Lodolo et al., 1993).

These reflectors are approximately parallel to the sea bottom and coincide with the depths predicted from phase diagrams. The sharp impedance contrast seen on the seismic profiles is believed to be the interface between sediments cemented with gas hydrate and underlying sediments with lower velocity due to the absence of hydrate and the possible presence of gas.

The dependence of bottom simulating reflectors on the temperature-pressure field, has been used to estimate geothermal gradients and heat flow in oceanic areas (Yamano et al., 1982; Davis et al., 1990; Kvenvolden and Kastner, 1990; Hyndman et al., 1992). In general, the estimated gradients and heat flow values are consistent with results obtained by direct measurements (Yamano and Uyeda, 1990). Ideally, calibration of the applicable stability field would be provided by a deep sea borehole that penetrated a clear bottom simulating reflector, with accurate down-hole temperature and sonic velocity measurements. This was attempted for the first time during ODP Leg 146 in the Cascadia Margin (Westbrook et al., 1994, personal communication).

The primary hydrate-forming gas in the seafloor is undoubtedly methane, generated from decomposition of buried micro-organic material at the depths where the hydrates occur, but

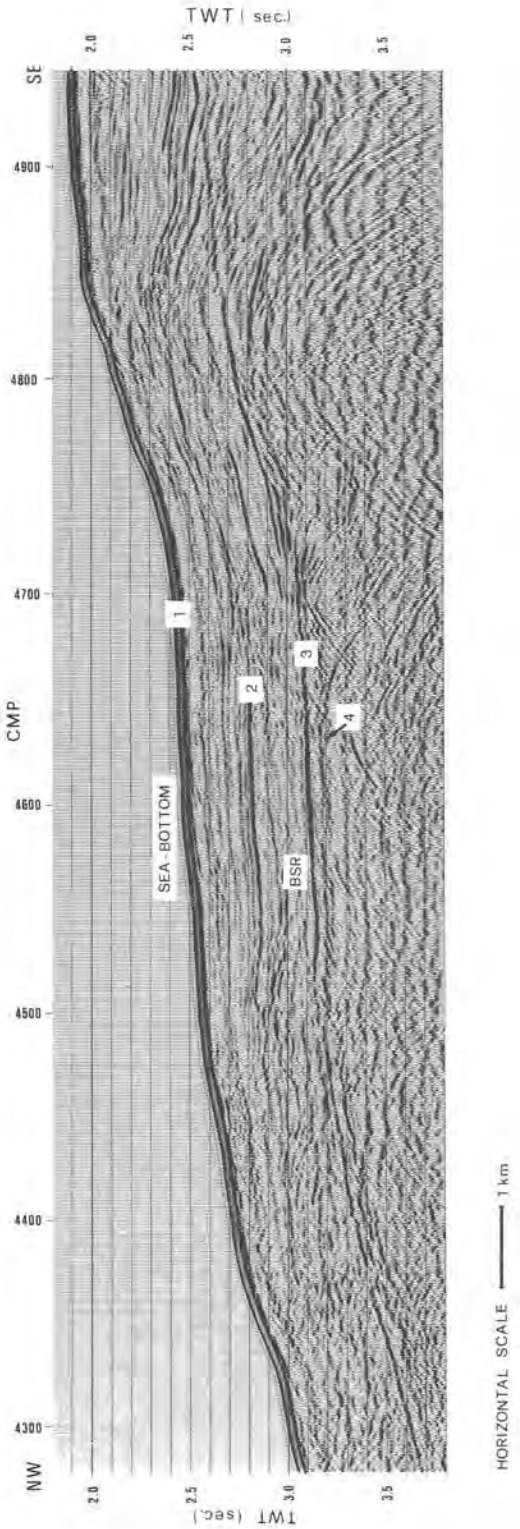

Fig. 5 - Portion of stacked seismic section of line IT9043 where the BSR is particularly evident. Numbers 1 to 4 on the profile indicate the horizons that have been picked for tomographic analysis.

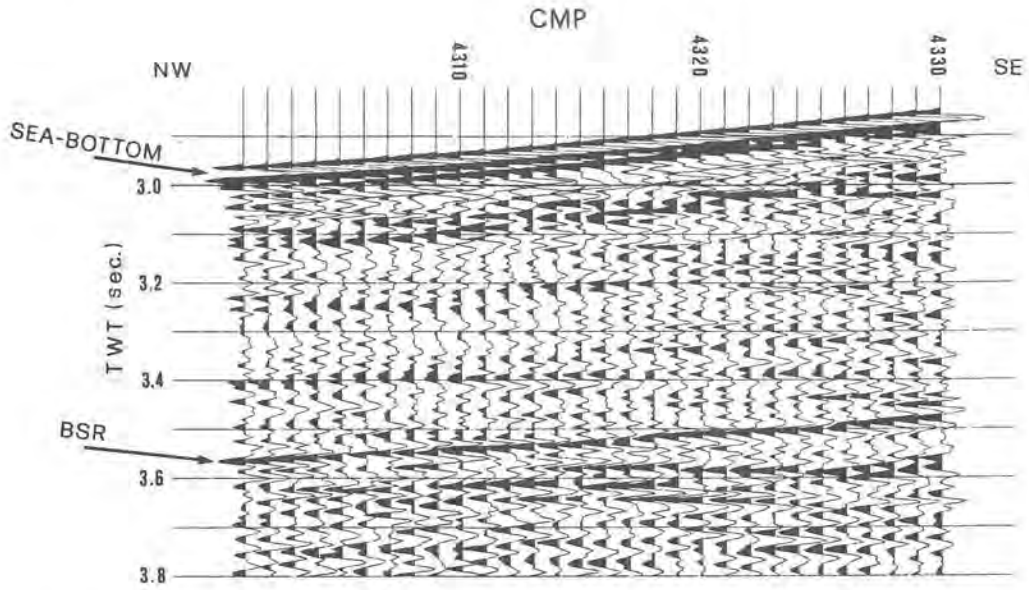

Fig. 6 - Relative amplitude display indicating the negative polarity of the BSR with respect to the seafloor.

the amount of organic matter present for the methane generation process is critical, and some mechanism for concentrating the methane seems required. A new model for hydrate formation was recently proposed by Hyndman and Davis (1992): they suggested a concentration mechanism, where BSR hydrate forms from dissolved biogenic methane carried upward in the rising fluid and swept out to form hydrates as it enters the stability field at the BSR. This mechanism is particularly efficient in subducting marine environments, where there is a sedimentary accretionary wedge.

Gas hydrates may have an economic role as a fossil fuel resource, both in the form of methane and of hydrogen, which can be extracted from the hydrate methane. Gas hydrates in shallow reservoirs can have more methane per unit volume than can be contained as free gas in the same space (Hunt, 1979). Theoretically, when appropriate hydrate expansion factors are considered, 1 m^3 of methane hydrate can contain up to 164 m^3 of methane gas under standard conditions. Kvenvolden and Grantz (1990) estimated that the total amount of gas in hydrate form may surpass the energy content of the total fossil fuel reservoirs by a factor of two. However, at present, there is only one example of commercial gas production from hydrates, the Siberian Messoyakha gas field which has been producing semi-continuously for the past 25 years (Sloan, 1990).

The methods used for production are today prohibitively expensive, and gas hydrates will become a potential energy resource when it can be shown that the energy required to release methane from the hydrate is significantly less than the thermal energy of the methane that can be recovered from the dissociated gas hydrate deposits.

Geologic hazards, particularly in marine environments, could be triggered by changes in pressure and temperature conditions on submarine gas hydrates that creates destabilization such as surficial slides and slumps on continental slopes, and several examples have been described in literature.

The most interesting aspect making gas hydrates a topical subject, from a global perspective, is their effect on global climatic change. The amount of methane trapped in gas hydrates onshore and offshore is about 3,000 times the amount in the atmosphere. Methane is both captured and released from gas hydrates, depending on the pressure-temperature regime; therefore, it can enter the atmosphere, and because it is a strong "greenhouse" gas, the methane from

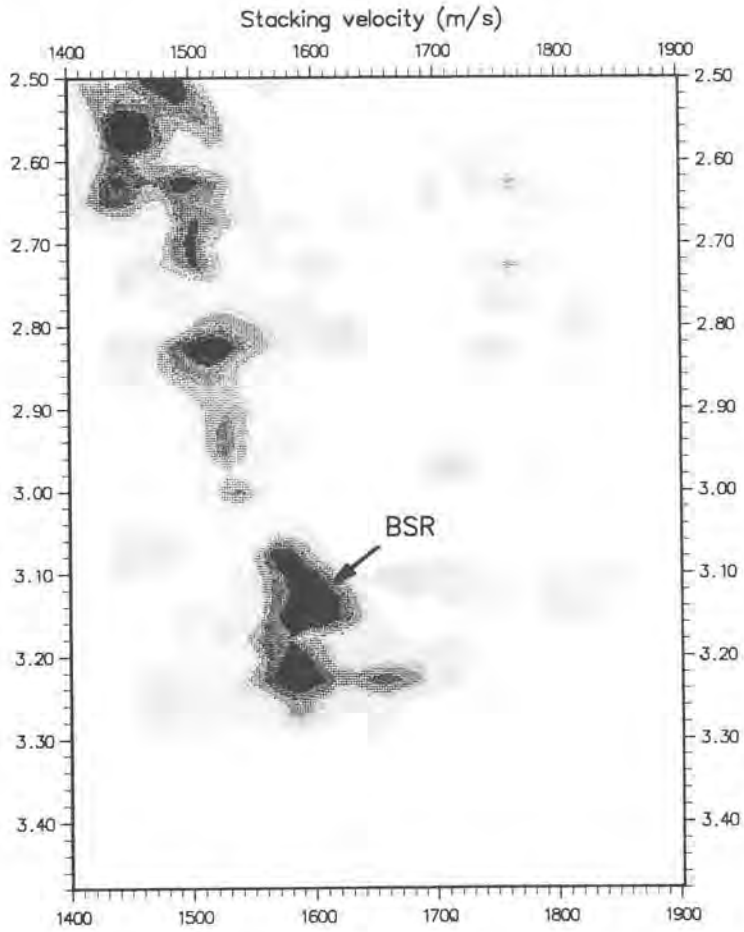

Fig. 7 - Conventional stacking velocity spectrum, displaying a velocity decrease at the BSR arrival time (arrow).

gas hydrates may influence global climate, past, present, and future (MacDonald, 1990). During global warming and cooling, that is during interglacial and glacial climates, gas hydrate deposits should respond to surface pressure and temperature changes, and in this context, many ideas have been proposed to explain the role of gas hydrates in past global climate change (see Nisbet, 1990; Paull et al., 1991).

THE BSR OF THE SOUTH SHETLAND MARGIN

The BSR identified on line IT9043 (Fig.5) is a well defined, high-amplitude and nearly continuous reflector. It is almost always a single symmetrical pulse, which indicates a simple interface (Hyndman and Spence, 1992).

The reflector crosses seismic horizons that reflect the position and orientations of sedimentary layers. It must therefore be younger than and superimposed on the acoustic structure of these sediments. The sub-bottom depth of the BSR generally increases with increasing water depth, and shows the characteristic relationship (Kvenvolden and McMenamin, 1980) of increasing hydrate stability zone thickness with increasing pressure. Local discontinuities of the reflector could be caused by structural discontinuities, discontinuous gas zones near the base of the hydrate stability zone, or ground water or gas chemistry variability that renders the base of the hydrate stability zone geometrically more complex than elsewhere.

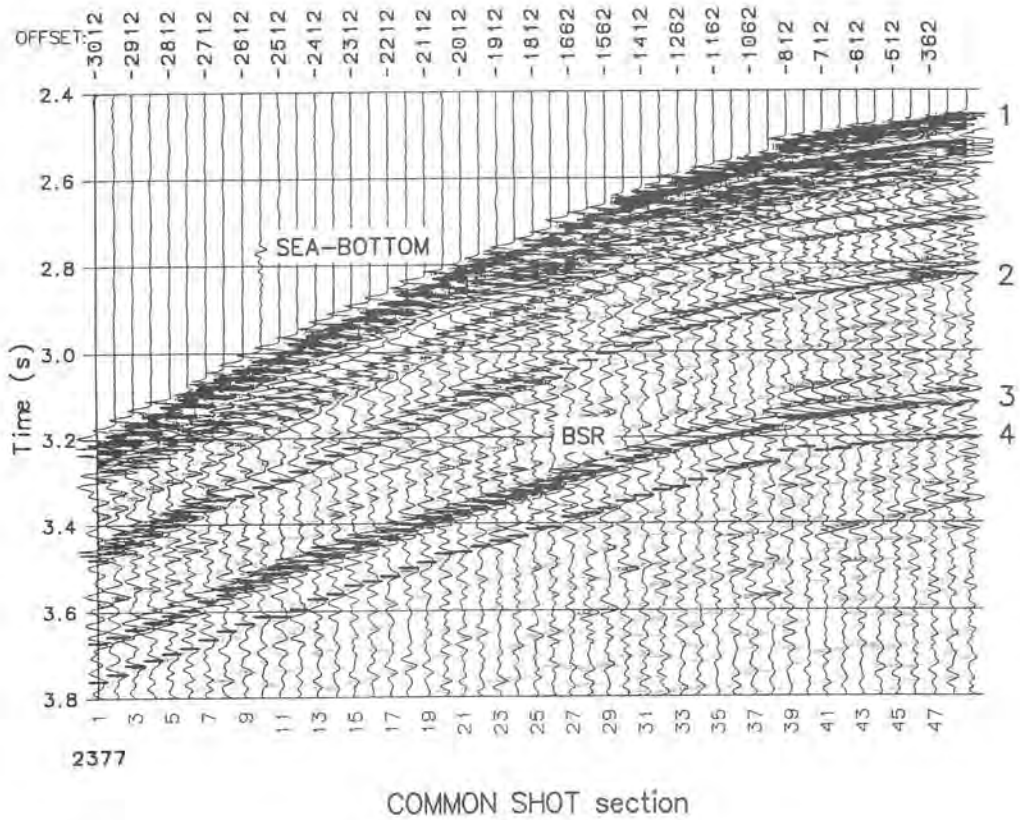

Fig. 8 - Picked traveltimes for the four considered horizons in a common shot gather.

The true amplitude display (Fig. 6) indicates a consistent negative polarity of the BSR with respect to the seafloor reflection. This is consistent with high acoustic velocity gas hydrate-saturated sediments, at least at the base of the hydrate stability zone, overlying lower velocity sediments in which free gas may be present.

The reflection coefficient of the seafloor, calculated by comparing the amplitude of the seafloor reflection with the amplitude of the seafloor multiple on near-normal incidence traces (to avoid complications from variations in amplitude with offset), gives values ranging from 35% to 40%. Because the amplitude of the BSR is about 50% of the primary seafloor reflection, we conclude that the reflection coefficient of the BSR must be large. Significant reflection coefficients (up to 50% of the seafloor) can be anticipated at a hydrate stability zone base/gas-rich contact.

The preliminary velocity analyses carried out over a short section where the BSR is strong, approximately flat, and the geological structure relatively uniform (from CMP 4500 to CMP 4650 on seismic line IT9043) showed that the hydrate layer is well resolved (Fig. 7), and the calculated interval velocity above it ranges from 2.0 to 2.2 km/s; just below this anomalous velocity gradient, the velocity rapidly decreases. Based on this velocity profile, we assume that the BSR is produced by a high velocity layer (sediments and hydrates) above a low velocity layer (sediments and free gas).

THE RESOLUTION REQUIRED

In this study we used the tomographic analysis in order to observe spatially organised variations

of the stacking velocities and provide a first approximation to the 2-D velocity distribution across the BSR of the South Shetland Margin.

Before introducing the techniques adopted in the tomographic analysis, we discuss methods and expected results in terms of resolution. This is motivated by the need to verify that the bottom simulating reflector of the South Shetland Margin is caused by a phase change in the fluids filling the sedimentary sequence, i.e. free gas is contained in the pore spaces below the reflector. We choose to assume a low-velocity zone below the reflector as indicated by the anomalous RMS velocity distribution (Lodolo et al., 1993). There are no rules for determining the thickness of a gas layer below a BSR. Hyndman and Spence (1992) conclude that below the BSR of the Vancouver margin (off the Pacific coast of Canada), gas if present must be thinner than a few meters, so that its presence cannot be revealed by the 50 m seismic wavelength available at that depth as a result of the earth's structure in that area and the acquisition parameters employed. In that case, the BSR was modelled with a simple layer of hydrate-bearing sediments overlying normal sediments.

In modelling the BSR of the Peru Margin, Miller et al. (1991) also pointed out that a gas layer thinner that 5.5 meters would not be detectable by multichannel seismic reflection techniques. However, a layer model with gas-bearing sediments 5.5-17 m thick simulates well the presence of the reflector in certain areas of higher amplitude.

Electrical logging and Vertical Seismic Profiling through the BSR of the Cascadia Margin (ODP Leg 146) indicate the thickness of the free gas zone to be at least 50 m and 15 m in the Oregon and Vancouver margins respectively (MacKay et al., 1994, personal communication).

According to laboratory tests (Pearson et al., 1986) and field measurements of compressional wave velocities (Domenico, 1974, 1976; Bangs et al., 1993), in sediments containing various brine-gas mixtures, about 80% of the total velocity decrease occurs abruptly for a gas content between 5% and 10%. In particular, the velocity of the sediment layer containing solid gas hydrates is of the order of 1800-2000 m/s, whilst in the underlying layer the velocity can be as low as 1300 m/s in the case of gas-rich sediments, and 1700-1900 m/s in the water-saturated layer, as calculated by Miller et al. (1991) for the gas hydrate zone found offshore Peru. Therefore, a noticeable velocity contrast occurs at the interface between the solid and liquid or gaseous transition of the saturating fluids.

A spectral analysis of the seismic arrivals from the BSR showed that the dominant frequency is of the order of 40 Hz. The corresponding wavelength at the target depth is about 50 meters. Since this length is generally larger than or approximately equal to the predicted anomaly thickness, we cannot expect to receive distinct and well resolved reflections from both the top and bottom of the inferred gas-saturated layer. In addition, amplitude interference may impede the signal recognition in the seismic sections.

THE AVAILABLE RESOLUTION

Conventional stacking velocity analysis is able to estimate RMS velocity with a sufficient accuracy (2-3%) if the layers are nearly horizontal and the incidence angles are small. In that case, we can simply apply Dix's formula to get the interval velocities, which is the information we need to identify anomalous variations of the wave velocity. This approach is certainly acceptable in the area comprised between CMP 4500 and 4650 of line IT9043 in Fig. 5, where the assumed BSR is flat and nearly horizontal, while it has to be taken with a grain of salt elsewhere.

Although the stacking velocity accuracy is sufficient (strictly speaking), we should note that the resolution in space and time of the velocity spectra is quite limited. In fact, a sort of spatial averaging over the acquisition spread, whose length in our case is 2670 m, is carried out in stacking velocity analysis. As a consequence, we are not able to directly measure sharp lateral velocity variations, but only to observe (and in some cases invert) the spatially organised oscillations induced in the continuous velocity spectra of the underlying horizons (Loinger, 1983; Harlan, 1989; Carlini et al., 1989).

Along the time dimension, the coherency values are averaged, usually within time windows

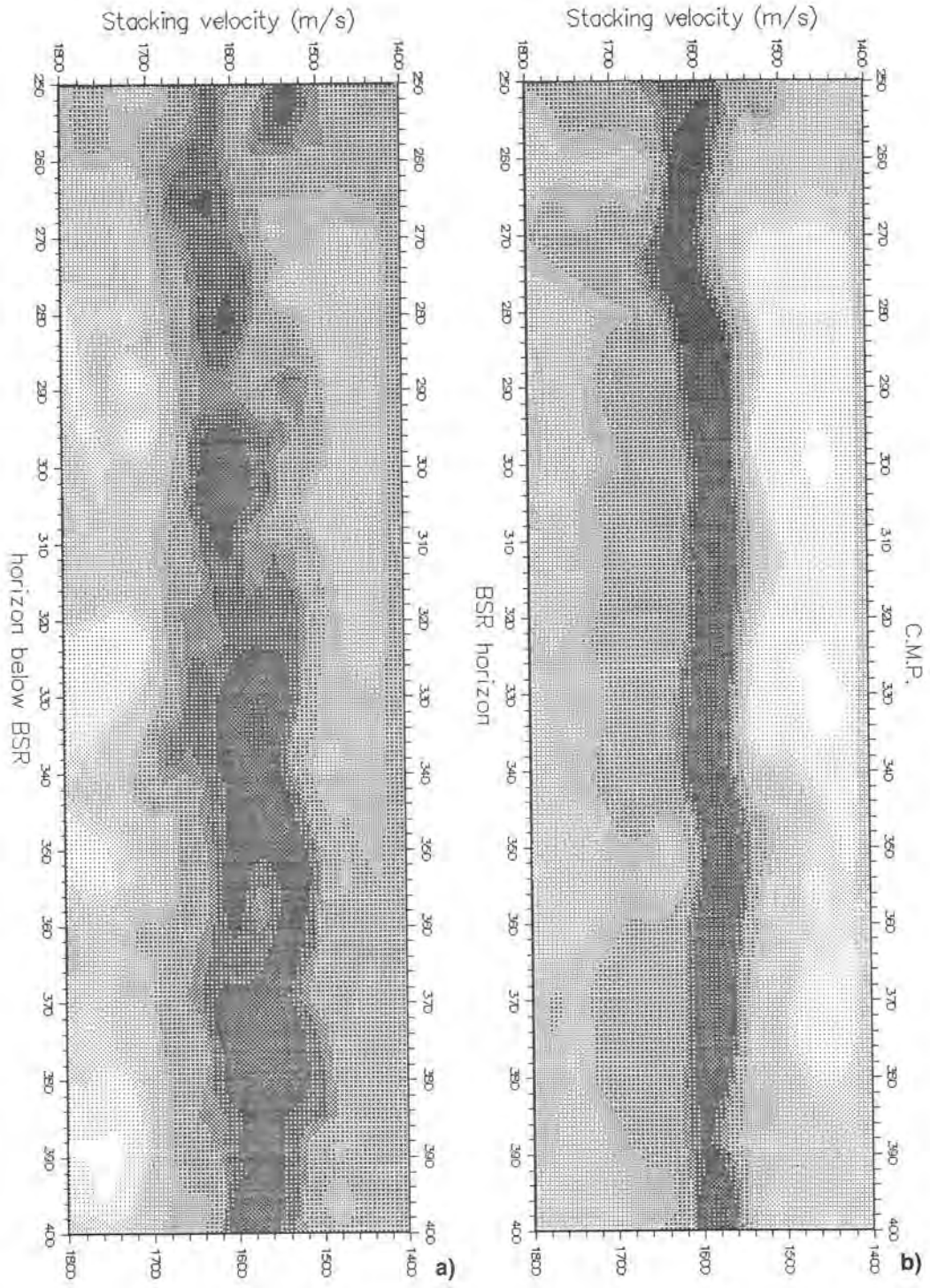

Fig. 9 - Continuous velocity spectra along the BSR (a), and the underlying horizon (b). The tomographic analysis was done between CMP 250 and 400, which corresponds to CMP 4490 and 4640 in Figs. 1, 2, 5 and 6.

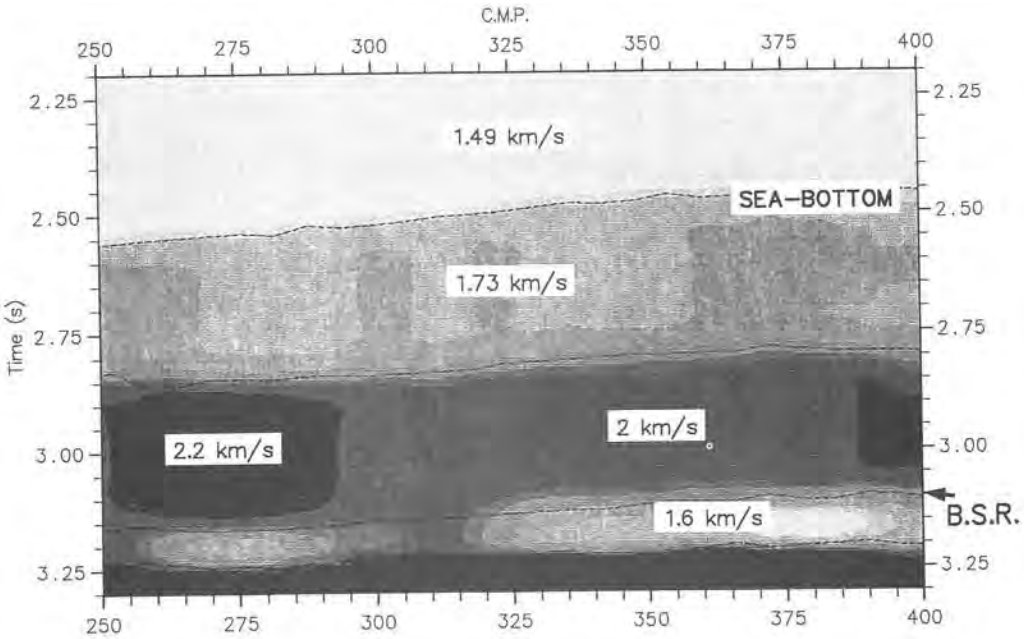

Fig. 10 - Interval velocity field obtained by picking the continuous velocity spectra.

whose length is comparable with that of the seismic wavelets. In our case, at the target depth, this length is about 40 ms, which means, converted in depth, about 50 meters. This figure is again larger than the anomaly sought, and could be a serious drawback: for this reason, we also considered using velocity spectra without time windows. Since the signal-to-noise ratio is good in the seismic data considered, this test produced fair results, but unfortunately not significantly different from those displayed above.

Seismic wavelets are band-limited signals, and therefore their direct comparison by semblance or cross-correlation in stacking velocity analysis necessarily provides a band-limited estimate. Tomographic inversion of traveltimes is able to significantly increase the resolution for two main reasons:

1. the picking of seismic reflections transforms them practically into point events;

2. there is no spatial average, since each event preserves its individual contribution to the velocity estimation during the whole inversion procedure.

For the first point, some caution is necessary: although the picking is a spiking process, which concentrates an event into a single point, the accuracy is limited by various causes such as the presence of noise, interference with other events, phase rotations at supercritical incidence angles, and so on. We have therefore to consider this point in a statistical sense, which means (as will be explained later) that some averaging is still necessary for our velocity estimate.

For the second point, the expected spatial resolution is of the order of the trace spacing, which is 25 meters in our case; this value is different by two orders of magnitude to that provided by stacking velocity analysis, which is of the order of the spread length.

When we evaluate the reliability of the velocity field given by the tomographic inversion, we have to also take into account the non-uniqueness of the tomographic solutions. Since the null space generally exists, the earth image provided by the dual tomography algorithm is probably the most reasonable available and compatible with the experimental data, but other solutions exist which satisfy the picked traveltimes as well.

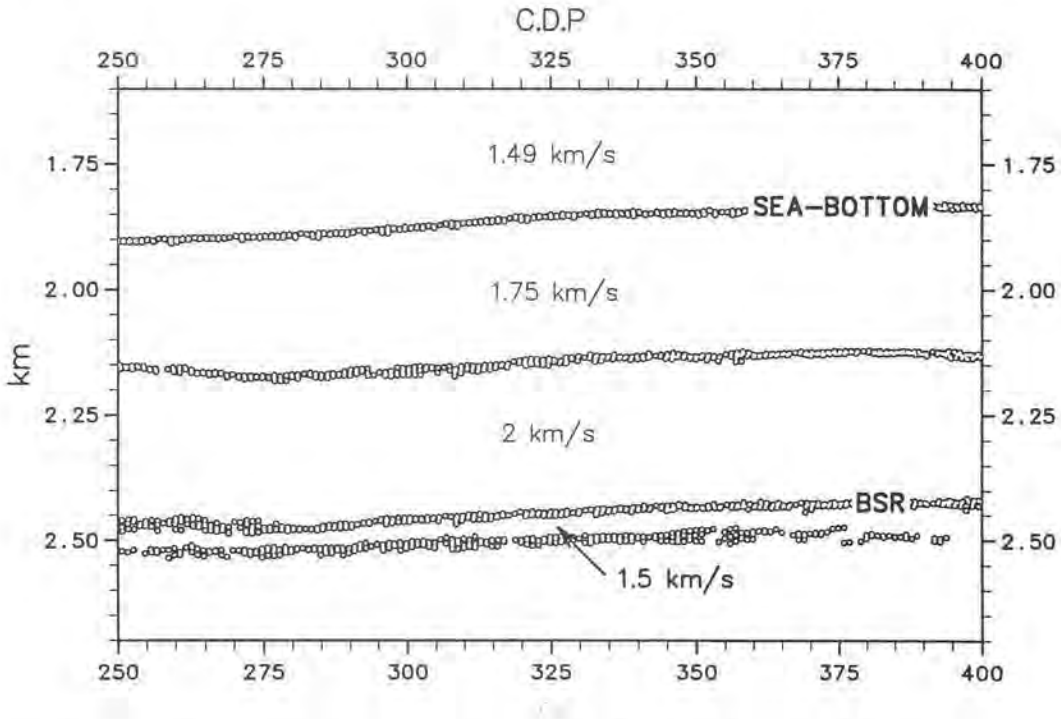

Fig. 11 - Best result provided by the tomographic inversion of reflected arrivals (velocity 1.5 km/s).

An additional ambiguity is due to the contemporary inversion of velocity and reflectors depth, if reflected arrivals are considered. Many of these uncertainties are removed by the procedure described in the next paragraph, but not all. Although a detailed theoretical discussion of this problem is beyond the scope of this paper, some synthetic examples illustrating this ambiguity are presented in the final part.

THE TOMOGRAPHIC INVERSION ALGORITHM

Probably we do not need to describe the conventional stacking velocity procedure (Taner and Koehler, 1969), and we refer the reader to the review by Sguazzero and Vesnaver (1987) for further details. The reflection tomography algorithm adopted here is described in detail by Carrion et al. (1993a, 1993b) and a direct comparison with stacking velocity analysis may be found in Boehm et al. (1993). Here we would like to recall briefly its basic concepts, which will useful for interpreting the velocity diagrams obtained and presented later.

The space is discretized by long pixels, which are zones where the propagation velocity of seismic waves is assumed to be constant. The pixel shapes may be quite irregular: their lateral boundaries are vertical straight lines, whilst the upper and lower ones coincide with the interpreted reflecting interfaces. This pixel shape is dictated by the resolution available with surface acquisition geometry, which gives a good estimate of the lateral gradients but is a poor one for the vertical variations comprised between two reflectors. In this way, a vertically averaged velocity is estimated between the upper and lower reflector.

The iterative inversion procedure can start with any initial model, which can also be very far from the true solution. Rays are traced to simulate the seismic wave propagation in the velocity field and reflector positions. The picked traveltimes are then compared with those simulated, and the differences obtained (the so-called residuals) are used to update the model. At each step, the velocity distribution is updated first, obtaining an estimate of the depth location

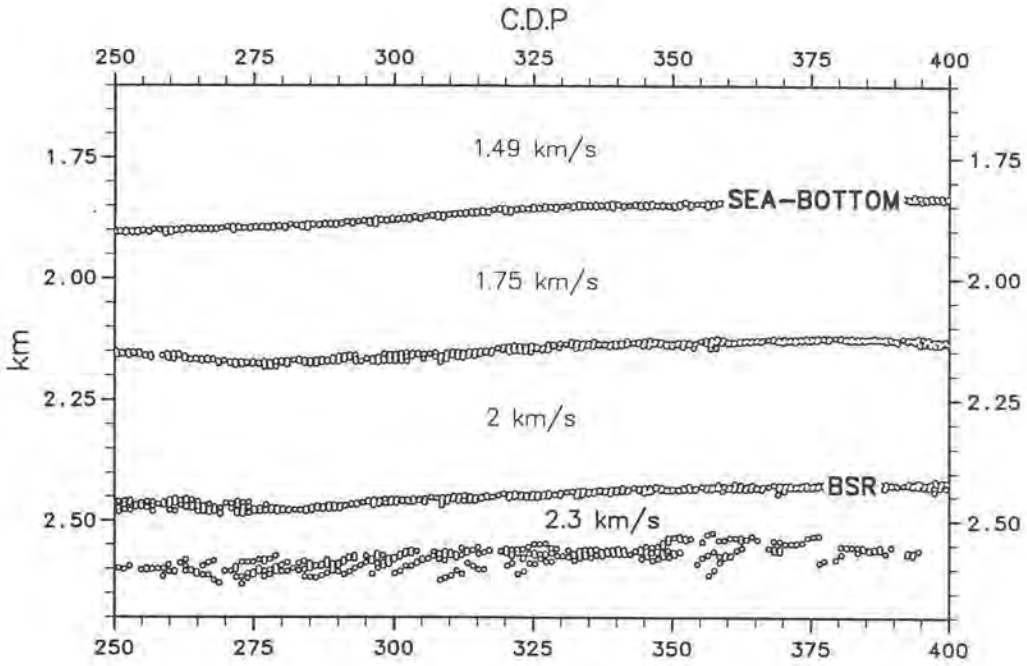

Fig. 12 - Using a velocity value of 2.3 km/s in the layer below the BSR, the dispersion in the estimated reflection points along the deepest horizon is large.

of the reflection point for each source-receiver position and for each reflector. Then, observing the pattern and the dispersion of these reflection points, a new estimate is made for the reflector structure and the local velocity changed; in fact, the possible presence of lateral velocity gradients is revealed by a spatially organised dip of reflection points as a function of the offset between source and receiver. The final solution is obtained iterating these two steps alternately, until a minimum dispersion is obtained for all reflectors.

The dual tomography algorithm (Carrion, 1991) converges rapidly to a stable solution, which is orthogonal to the null space of the tomographic matrix. This mathematical result stems from the choice of an object function which is different from the conventional one, the energy of traveltime residuals. In the Carrion's approach, the energy of the velocity distribution in the pixels is minimised instead, whilst the picked traveltimes are introduced in the problem as constraints. As a spin-off, we get a velocity field which is quite smooth and dependent on the initial model only where (too) few significant events contribute to the inversion process, and has excellent resolution and stability elsewhere. This means that the smoothness of our solution does not need to be forced to stabilize the estimated velocity field, so compromising the resolution of the depth image.

VELOCITY ANALYSIS RESULTS

Conventional velocity spectra give an estimate of the vertical velocity changes. To check the lateral extent of the interval velocity decrease, we generated four continuous velocity spectra along four horizons picked on the stacked section of line IT9043 (see Fig. 5), and were considered the four most continuous and reflective seismic horizons identified, as shown in a common shot gather (Fig. 8). Horizon 1 corresponds to the sea-bottom; horizon 2 is at an intermediate depth between the primary reflection and the BSR (referred to as horizon 3). According to our interpretation, horizon 2 corresponds to a lithologic change in the layered slope sedimentary cover. Horizon 4 is a less continuous, but consistent horizon found immediately below the BSR.

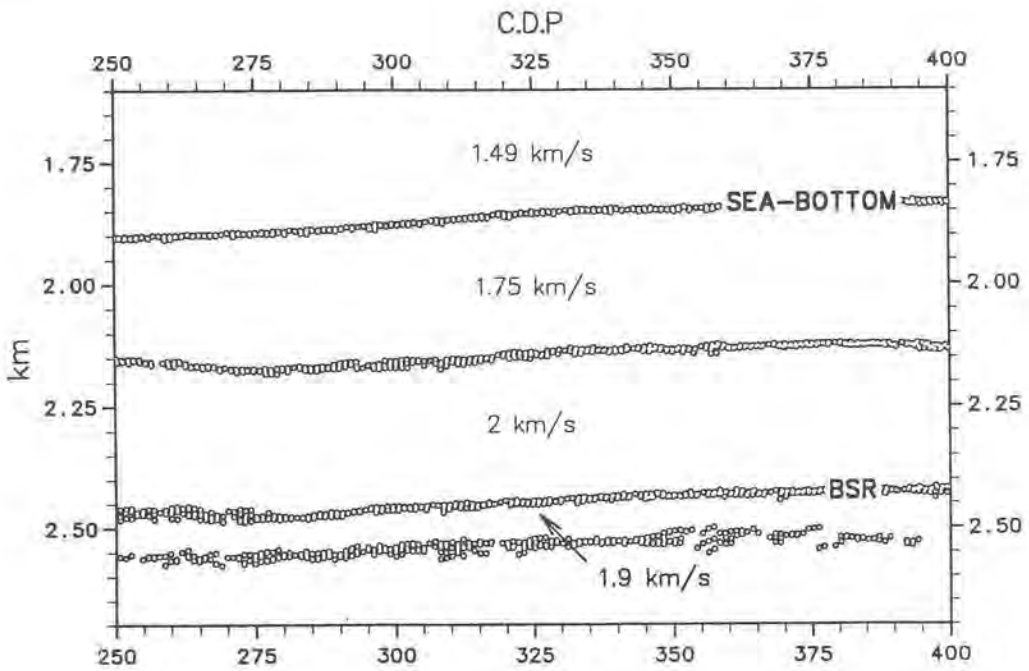

Fig. 13 - Using a velocity value of 1.9 km/s in the layer below the BSR, the dispersion in the estimated reflection points along the deepest horizon is larger than that in Fig. 11.

The signal coherency was measured using the normalised complex cross-correlation, which provides a better resolution with respect to the semblance or other coherency estimators (Sguazzero and Vesnaver, 1987). As shown in Fig.9a, we got very sharp and spatially continuous coherency maxima at about 1600 m/s for the BSR; similar velocity values are suggested for the underlying horizon, whose spectrum is more confused because its reflected energy is much weaker (Fig. 9b).

In Fig. 10 we see the interval velocity field produced by the continuous velocity spectra. A clear velocity decrease may be noticed at the arrival time of the BSR, along the whole CMP interval; its two-way time duration of about 80 ms corresponds, in depth, to 60-70 m.

A pre-stack picking of the four selected horizons was carried out to invert the traveltimes of the reflected arrivals (Figs. 11, 12 and 13). As seen in all these figures, the average local velocity of the layers above the BSR is reliable, since the dispersion of the estimated reflection point is small. In Fig. 11, a value of 1.5 km/s just below the BSR produces a substantially well-resolved reflector, and the dispersion is quite low; attempts to vary this velocity by 10% did not produce observable changes in the point dispersion. We can totally exclude for that layer a velocity as high as 2.3 km/s, because it produces a large dispersion (Fig. 12), and we may confidently set the velocity 1.9 km/s as the upper limit for acceptable values in this area (Fig. 13), since approaching this value we begin to notice a larger dispersion in the fourth horizon, in particular close to CMP's 260, 315, 355 and 375.

In general, in real data, the noise level can be high, local inhomogeneities exist in the velocity field, and mispicks may occur during the pre-stack picking, especially at large offsets and depths. All these factors may compromise the tomographic inversion's quality and reliability. A further test was therefore carried out to verify if the results obtained from real data are significantly affected by such problems, or if the precision limits of the velocity estimate in the layer below the BSR are due only to other factors, such as the acquisition geometry, the earth model adopted, and the velocity field itself. We simulated the reflected arrivals from a model composed of four homogeneous layers, with the same propagation velocities computed from the real data. The ray tracing program provided the travel times directly, so that no picking errors are possible.

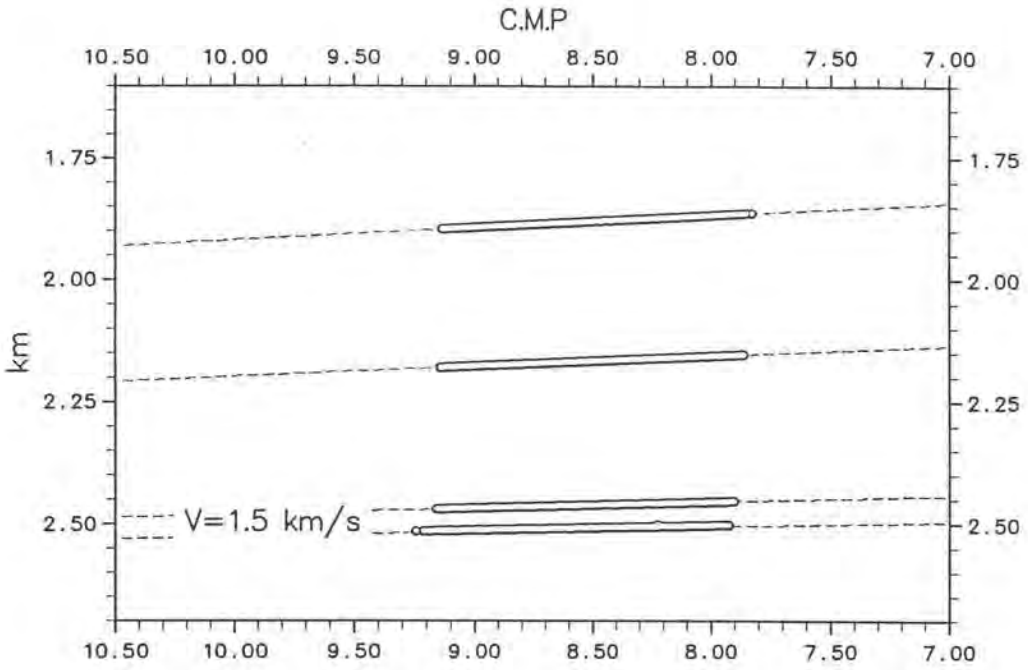

Fig. 14 - Tomographic inversion of the synthetic data, using the true velocities.

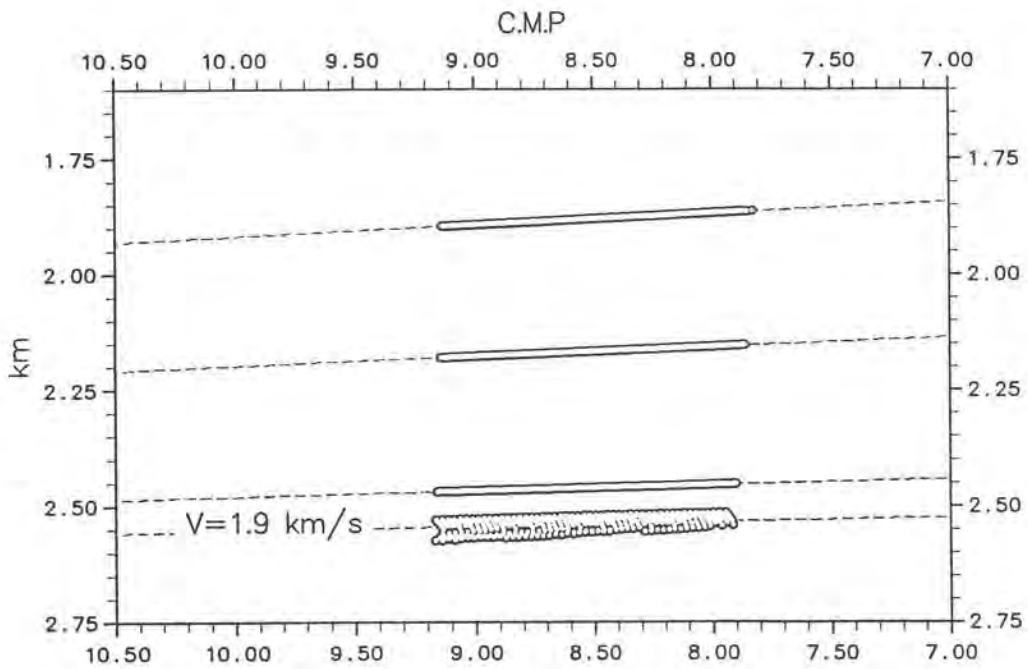

Fig. 15 - Tomographic inversion of the synthetic data, using the true velocities except in the third layer.

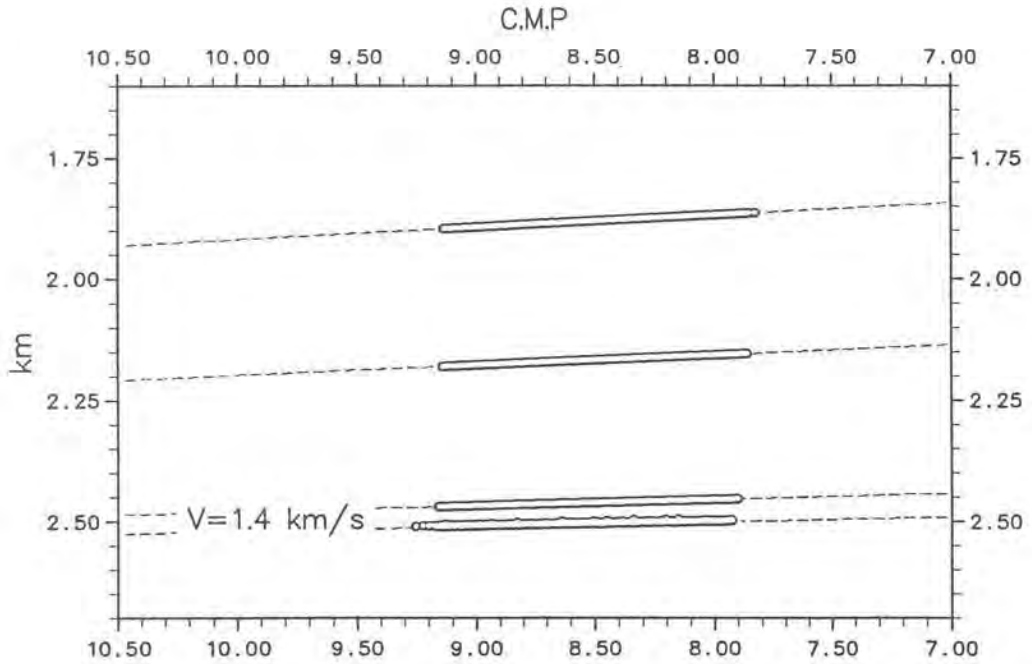

Fig. 16 - Tomographic inversion of the synthetic data, using the true velocities except in the third layer.

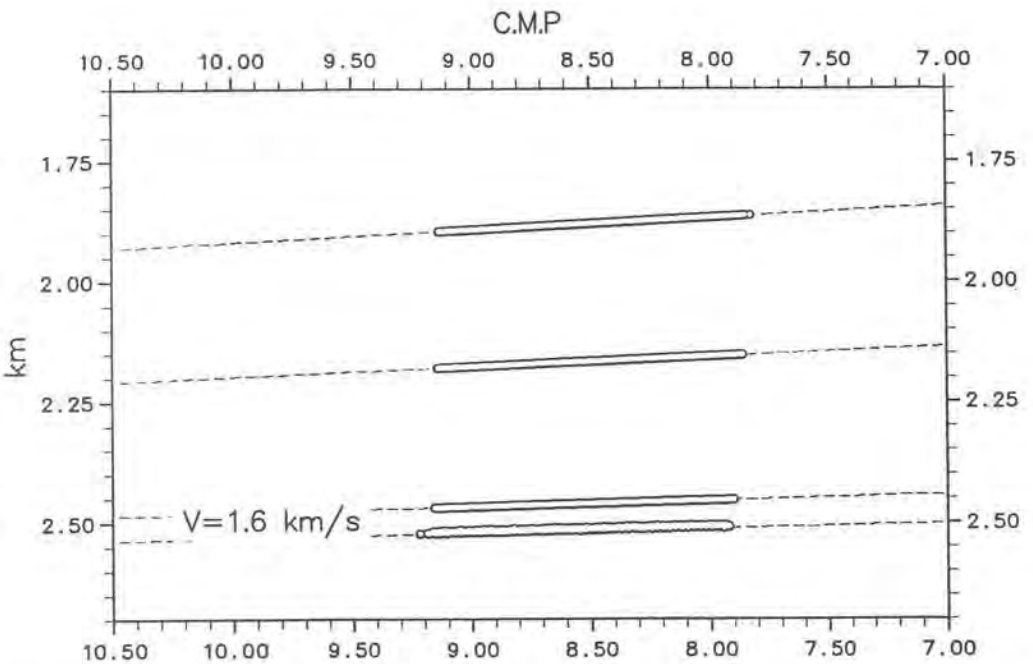

Fig. 17 - Tomographic inversion of the synthetic data, using the true velocities except in the third layer.

The tomographic inversion using the true velocities obviously provides the best result (Fig. 14), in terms of dispersion of the estimated reflection points, which is the same for all reflectors, and is optimum in particular for the fourth. If a larger value, such as 1.9 km/s, is used, a noticeably larger dispersion is observed (Fig. 15), and we can certainly exclude it from the acceptable solutions. On the other hand, we also see in this synthetic case that velocities slightly lower (Fig. 16) or higher (Fig. 17) than 1.5 km/s do not produce clear differences in dispersion. This confirms that the precision of the tomographic estimate is around $\pm 10\%$ of 1.5 km/s in this case, i.e., at this depth, with this global and local velocity distribution and with a conventional acquisition geometry.

CONCLUSIONS

Tomographic inversion analysis done on the multichannel seismic reflection profile across the accretionary prism of the South Shetland Margin confirms the presence of a strong bottom simulating reflector that had previously been recognized with conventional seismic analysis (Lodolo et al., 1993).

The inversion of the reflected arrivals from a layered model composed of four homogeneous horizons, identified on stacked seismic profile IT9043, allowed us to identify the 2-D velocity structure across the sedimentary cover, where the bottom simulating reflector is particularly strong. Below the reflector is a low velocity zone with average interval velocity of 1500 m/s $\pm 10\%$; above the reflector the sediments are characterized, with confidence, by a interval velocity ranging from 2000 to 2200 m/s.

The low velocity layer identified at about 800 m below the seafloor is probably produced by gas-bearing sediments. However, the limits of the resolution of the seismic data do not allow us to estimate its thickness. Qualitatively, the observed negative velocity anomaly could be produced either by a thin layer of extremely low velocity or by a thicker layer of less pronounced low velocity, or by various combinations.

As emerged from both general theoretical criteria and some *ad hoc* modeling and inversion tests, the resolution of the data is such that full confidence about the hypothesis that gas hydrates are present above the reflector is not possible. We can simply state that the average interval velocity found in the layer picked above the BSR is compatible with that of hydrate-bearing sediments, but we cannot comment on the thickness, lateral continuity, and concentration of the inferred hydrates.

It should also be noted that it is difficult to gain much more resolution from seismic data. The high frequency components in the source signature, even with a significant increase in the energy, would be reduced by anelastic absorption along their propagation path. Therefore, it is considered difficult to image both upper and lower interfaces of the velocity structure associated to the BSR in a seismic section.

Within these reliability limits, nevertheless, we may say that conventional and tomographic velocity analyses support the interpretation of the BSR as being due to a phase transition of pore fluids from solid to liquid or gaseous status, because of the clear spatial continuity of the reflectors and the related velocity decrease estimated independently with two totally different methods. In particular, tomographic inversion provides a depth reconstruction of the BSR with a resolution approximating theoretical limits; at the same time, the estimated thickness and velocity values are in the range of those measured in wells penetrating the gas hydrate layers.

Acknowledgement. The 1989-90 data acquisition campaign and the basic processing at OGS were funded by PNRA (Programma Nazionale di Ricerche in Antartide).

REFERENCES

Andreassen K., Hogstad K. and Berteussen K.A.; 1990: *Gas hydrate in the southern Barents Sea, indicated by a shallow seismic anomaly*. First Break, **8**, 235-245.

Bangs N.L.B, Sawier D.S. and Golovchenko X.; 1993: *Free gas at the base of the gas hydrate zone in the vicinity of the Chile triple junction*. Geology, **21**, 905-908.

Barker P.F.; 1982: *The Cenozoic subduction history of the Pacific margin of the Antarctic Peninsula: ridge crest-trench interaction*. Journal of Geol. Soc. London, **139**, 787-801.

Boehm G., Carcione J. and Vesnaver A.; 1993: *Conventional and tomographic velocity analysis applied to acoustic seismic models*. Atti del XII Convegno GNGTS, Roma, 1993, in press.

Camerlenghi A. and Lodolo E.; 1994: *Bottom simulating reflector on the South Shetland Margin (Antarctic Peninsula) and implications for the presence of gas hydrates*. Terra Antartica, **1**, 154-157.

Carlini A., Vesnaver A., Boehm G. e Harlan W.; 1989: *Inversione tomografica di anomalie nella velocità di Stack*. Atti del VIII Convegno GNGTS, Roma, 1989, 695-704.

Carrion P.; 1991: *Dual tomography for imaging complex structures*. Geophysics, **56**, 1395-1404.

Carrion P., Vesnaver A., Boehm G. and Pettenati F.; 1993a: *Aperture compensation tomography*. Geophysical Prospecting, **41**, 367-380.

Carrion P., Boehm G., Marchetti A., Pettenati F. and Vesnaver A.; 1993b: *Reconstruction of lateral gradients from reflection tomography*. Journal of Seismic Exploration, **2**, 55-67.

Carson B., Westbrook G., et al.; in press: Proc. ODP, Init.Repts., 146: College Station, TX (Ocean Drilling Program).

Collins B.P. and Watkins J.S.; 1985: *Analysis of a gas hydrate off southwest Mexico using seismic processing techniques and Deep Sea Drilling Project Leg 66 results*. Geophysics, **50**, 16-24.

Davis E.E., Hyndman R.D. and Villinger H.; 1990: *Rates of fluid expulsion across the northern Cascadia accretionary prism: constraints from new heat flow and multichannel seismic reflection data*. J. Geophys. Res., **95**, 8869-8889.

Domenico S.N.; 1974: *Effect of water saturation on seismic reflectivity of sand reservoirs encased in shale*. Geophysics, **39**, 759-769.

Domenico S.N.; 1976: *Effect of brine-gas mixture on velocity in an unconsolidated sand reservoir*. Geophysics, **41**, 882-894.

Gambôa L.A.P. and Maldonado P.R.; 1990: *Geophysical investigations in the Bransfield Strait and in the Bellingshausen Sea - Antarctica*. In: Antarctica as an exploration frontier - Hydrocarbon Potential, Geology, and Hazard, St. John B. (Ed.), AAPG Studies in Geology, **31**, 127-141.

González-Ferran O.; 1985: *Volcanic and tectonic evolution of the northern Antarctic Peninsula - Late Cenozoic to Recent*. Tectonophysics, **114**, 389-409.

Guterch A., Grad M., Janik T., Perechuc E. and Pajchel J.; 1985: *Seismic studies of the crustal structure in West Antarctica 1979-1980 - Preliminary results*. Tectonophysics, **114**, 411-429.

Harlan W.; 1989: *Tomographic estimation of seismic velocities from reflected raypaths*. Expanded Abstracts of 59th SEG Meeting, Dallas, 922-924.

Hawkes D.D.; 1981: *Tectonic segmentation of the northern Antarctic Peninsula*. Geology, **9**, 220-224.

Hitchon B.; 1974: *Occurrence of natural gas hydrates in sedimentary basins*. In: Natural gases in marine sediments, Kaplan I.R. (Ed.), Plenum Press, New York, 195-225.

Hunt J.M.; 1979: *Petroleum geochemistry and geology*, W.H. Freeman, San Francisco, 617 pp.

Hyndman R.D, Foucher J.P., Yamano M., Fisher A. and Scientific Team of ODP Leg 131; 1992: *Deep sea bottom simulating reflectors: calibration of the base of the hydrate stability field as used for heat flow estimates*. Earth and Planetary Sciences Lett., **109**, 289-301.

Hyndman R.D. and Davis E.E.; 1992: *A mechanism for the formation of methane hydrate and seafloor bottom simulating reflectors by vertical fluid expulsion*. J. Geophys. Res., **97**, 7025-7041.

Hyndman R.D. and Spence G.D.; 1992: *A seismic study of methane hydrate marine bottom simulating reflectors*. J. Geophys. Res., **97**, 6683-6698.

Kvenvolden K.A.; 1993: *Gas hydrates - Geological perspective and global change*. Reviews in Geophysics, **31**, 173-187.

Kvenvolden K.A. and Grantz A.; 1990: *Gas hydrates of the Arctic region*. In: The Arctic ocean region, Grantz A. Johnson L. and Sweeney J.F. (Eds.), GSA Decade of North American Geology, 539-549.

Kvenvolden K.A. and Kastner M.; 1990: *Gas hydrates of the Peruvian outer continental margin*. In: Proc. of the Ocean Drilling Program, Scientific Results, **112**, 517-526.

Kvenvolden K.A. and McMenamin M.A.; 1980: *Hydrates of natural gas: a review of their geological occurrence*. U.S. Geological Survey Circular No. 825, 11 pp.

Larter R.D. and Barker P.F.; 1991: *Effects of ridge crest-trench interaction on Antarctic-Phoenix spreading: forces on a joung subducting plate*. J. Geophys. Res., **96**, 19, 583-19, 607.

Lodolo E. e Camerlenghi A.; 1992: *Evidenze sismiche di gas idrati lungo il Margine Pacifico della Penisola Antartica*. Atti del XI Convegno GNGTS, Roma, 873-879.

Lodolo E., Camerlenghi A. and Brancolini G.; 1993: *A bottom simulating reflector on the South Shetland Margin, Antarctic Peninsula*. Antarctic Science **5** (2), 207-210.

Loinger E.; 1983: *A linear model for velocity anomalies*. Geophysical Prospecting **31**, 98-118.

MacDonald G.T.; 1990: *Role of methane clathrates in past and future climates.* Clim. Change, **16**, 247-281.

MacKay N.E., Jarrard R.D., Westbrook G.K., Hyndman R.D. et al.; in press: *Origin of bottom simulating reflectors: geophysical evidence from the Cascadia accretionary prism.* Geology.

Miller J.J., Lee M.W. and von Huene R.; 1991: *An analysis of a seismic reflection from the base of a gas hydrate zone, offshore Peru.* AAPG Bulletin, **75**, 910-924.

Minshull T. and White R.; 1989: *Sediment compaction and fluid migration in the Makran accretionary prism.* J. Geophys. Res., **94**, 7387-7402.

Nisbet E.G.; 1990: *The end of ice age.* Can. Jour. Earth Sci., **27**, 148-157.

Paull C.K., Ussler III W. and Dillon W.P.; 1991: *Is the extent of glaciation limited by marine gas hydrates?.* Geophys. Res. Lett., **18**, 432-434.

Pearson C., Murphy J. and Hermes R.; 1986: *Acoustic and resistivity measurements on rock samples containing tetrahydrofuran hydrates: laboratory analogues to natural gas hydrate deposits.* J. Geophys. Res., **91**, 14, 132-14, 138.

Pelayo A.M. and Wiens D.A.; 1989: *Seismotectonics and relative plate motions in the Scotia Sea region.* J. Geophys. Res., **94**, 7293-7320.

Sguazzero P. and Vesnaver A.; 1987: *A comparative analysis of algorithms for seismic velocity estimation.* In: 'Deconvolution and Inversion ', Bernabini et al. (eds), Blackwell, Oxford, United Kingdom, 267-286.

Shipley T.H. and Didyk B.M.; 1981: *Occurrence of methane hydrate offshore southern Mexico.* In: Watkins J.S., Moore J.C. et al., Init. Repts. DSDP, 66: Washington (U.S. Govt. Printing Office), 547-555.

Shipley T.H., Houston M.H., Buffler R.T., Shaub F.J., McMillen K.J., Ladd J.W. and Worzel J.L.; 1979: *Seismic evidence for widespread possible gas hydrate horizons on continental slopes and rises.* AAPG Bull., **63**, 2204-2213.

Sloan E.D.; 1990: *Clathrate hydrates of natural gases.* Marcel Dekker, New York, 464-474.

Taner M.T. and Koehler F.; 1969: *Velocity spectra - Digital computer derivation and applications of velocity functions.* Geophysics, **34**, 859-881.

Yamano M. and Uyeda S.; 1990: *Heat-flow studies in the Peru Trench subduction zone.* In: Suess E., von Huene R. et al., 1990. Proc. ODP, Sci. Results, 112: College Station, TX (Ocean Drilling Program), 653-661.

Yamano M., Uyeda S., Aoki Y. and Shipley T.H.; 1982: *Estimates of heat flow derived from gas hydrates.* Geology, **10**, 339-343.